THE ASTROPHYSICAL JOURNAL, 558:702–716, 2001 September 10

SEARCHING FOR AMMONIA IN GRAIN MANTLES TOWARD MASSIVE YOUNG STELLAR OBJECTS

E. L. GIBB[1] AND D. C. B. WHITTET[1]
Department of Physics, Applied Physics and Astronomy, Rensselaer Polytechnic Institute, Troy, NY 12180
AND
J. E. CHIAR[2]
NASA-Ames Research Center, Mail Stop 245-3, Moffett Field, CA 94035
Received 2001 February 20; accepted 2001 May 10

ABSTRACT

We present a study of the mid-infrared spectral regions of 17 objects observed with the Short-Wavelength Spectrometer on the *Infrared Space Observatory* (*ISO* SWS) in a search for the presence of the elusive NH_3 solid-state absorption features at 2.96 and 9.0 μm. We compare the 3 μm profile with laboratory spectra of pure water and water/ammonia mixtures from the Leiden Molecular Astrophysics database. We determine that the shape of the 3 μm water feature alone does not present conclusive evidence of the presence or lack of NH_3 ice on dust grain mantles because of the large number of unknown physical parameters that influence the 3 μm water profile: grain size distribution, grain shape, mantle composition, thermal history, and geometrical effects. In the 9 μm region, the presence of NH_3 is characterized by a sudden change in slope at 8.5 μm and a peak at 9.0 μm within the silicate profile. Of the 16 silicate features studied, four show evidence of a 9 μm ammonia feature, including the previously reported detections in ground-based observations of NGC 7538 IRS 9, and SWS observations of W33 A. Upper limits are found for the remaining objects. Why NH_3, which is an abundant gas-phase molecule in cold, dense cores, is not apparently present in significant amounts on most grain mantles, where it is expected to freeze out, is currently a mystery.

Subject headings: infrared: ISM — ISM: abundances — ISM: molecules — line: profiles

1. INTRODUCTION

Infrared spectra of young stellar objects (YSOs) embedded within cold, dark molecular clouds show solid-state absorption features characteristic of simple molecules presumed to exist as ice mantles on silicate cores of dust grains. Spectral features found in these YSOs include vibrational modes of H_2O, CO, CO_2, OCS, CH_3OH, CH_4, and "XCN" (a CN-bearing species that has yet to be firmly identified). The characteristics of these features (width, shape, and depth) provide a diagnostic of the thermal and radiative history and the chemical composition along the line of sight. In order to understand the chemical and physical evolution of dark clouds and star formation regions, we must study the composition and structure of ice mantles and silicate cores in varying environments.

Nitrogen is an abundant element and is expected to contribute to the presence of ice mantles in cold, dark clouds. Much of this nitrogen may be in the form of N_2, which is infrared inactive and hence very difficult to detect. When frozen in nonpolar ices, it has a weak vibrational mode at 4.296 μm, which is completely obscured by the long-wavelength wing of the 4.27 μm CO_2 feature (Elsila, Allamandola, & Sandford 1997). Nitrogen is known to exist in the XCN feature at 4.62 μm, and NH_3 is the N carrier for laboratory production of XCN by UV photolysis (Bernstein et al. 1995). Cyanates are currently the prime candidate for this feature (X—O—C≡N; Schutte & Greenberg 1997; Gibb et al. 2000; Whittet et al. 2001). However, a firm identification has not yet been made (Pendleton et al. 1999).

Gas-phase ammonia has been known in molecular clouds for several decades. It is used as a tracer of star formation, since its inversion transitions in the metastable rotational levels are observed in regions where the density exceeds $n \gtrsim 10^4$ cm^{-3} (Taylor, Morata, & Williams 1998) and the ratios of the line intensities are sensitive to the gas temperature. Observations of NH_3 gas in cold (10 K), dense cores reveal $N(NH_3) \approx 10^{14}$–10^{15} cm^{-2} (Federman, Huntress, & Prasad 1990), corresponding to $N(NH_3)/N(H_2) = 3 \times 10^{-8}$–$2 \times 10^{-7}$ cm^{-2}. Ammonia is expected to form in cold clouds via a sequence of gas-phase reactions such as

$$N + H_3^+ \rightarrow NH_2^+ + H\,, \quad (1)$$

$$NH_2^+ + H_2 \rightarrow NH_3^+ + H\,, \quad (2)$$

$$NH_3^+ + H_2 \rightarrow NH_4^+ + H\,, \quad (3)$$

$$NH_4^+ + e^- \rightarrow NH_3 + H \quad (4)$$

(Scott, Freeman, & McEway 1997). Many authors cite the first reaction as

$$N^+ + H_2 \rightarrow NH^+ + H\,, \quad (5)$$

followed by

$$NH^+ + H_2 \rightarrow NH_2^+ + H \quad (6)$$

(Le Bourlot 1991), but experiments have shown that reaction (5) is endothermic and critically dependent on the ortho to para ratio of molecular hydrogen. The reaction can only occur in dark molecular cloud conditions [$T \approx 10$ K, $n(H_2) \approx 10$ cm^{-3}] when the ortho/para ratio is greater than a few times 10^{-4} (Marquette et al. 1985; Le Bourlot 1991). At these low temperatures, ammonia should efficiently freeze onto ice mantles and would be expected to be completely in the solid phase within a few hundred years in the absence of nonthermal desorption mechanisms (Sandford & Allamandola 1993).

Another possible mechanism for NH_3 formation involves grain surface catalysis, which is characterized by a high

[1] New York Center for Studies on the Origins of Life, Rensselaer Polytechnic Institute, Troy, NY 12180.
[2] SETI Institute, Mountain View, CA 94043.

abundance of saturated species. At cold (10 K) temperatures found in dark clouds, most species are expected to freeze on the grain in a short period of time. Atomic nitrogen on the surface would react with migrating hydrogen atoms to form NH_3. If NH_3 is present in the dust mantles, it should evaporate at the temperatures exceeding ~ 50 K found in hot cores, resulting in an abundance peak in warm regions. The large gas-phase NH_3 abundances relative to hydrogen [$\sim(1\text{–}10) \times 10^{-6}$] reported for several hot cores and ultracompact H II regions such as G34.3+0.15 (Heaton, Little, & Bishop 1989), OMC-1 (Blake et al. 1987), and G9.62+0.19, G29.96−0.02, G10.47+0.03, and G31.41+0.31 (Cesaroni et al. 1994) support this.

In the solid phase, NH_3 has three infrared active vibrational modes: an NH stretch at 2.963 μm (3375 cm^{-1}), NH deformation at 6.158 μm (1624 cm^{-1}), and an inversion mode at 9.346 μm (1070 cm^{-1}), which laboratory data have shown to shift to 9.0 μm in a polar (H_2O-rich) mixture. These transitions are difficult to detect, since they are all blended with the much stronger absorption features of the water stretching and bending modes at 3.1 and 6.0 μm, respectively, and the broad silicate feature at 9.7 μm.

There has been much discussion in the literature about the presence or lack of the ammonia feature at its 2.96 μm position. Knacke et al. (1982) claimed a column density of 1×10^{18} cm^{-2} in Orion BN, or about 25% that of water, a claim that was later retracted by Knacke & McCorkle (1987). A later paper by Smith, Sellgren, & Tokunaga (1989) showed that the shape of the 3 μm H_2O profile of BN could be adequately fitted by pure water run through a MRN (Mathis, Rumpl, & Nordsieck 1977) scattering model. The best fit was for a 23, 77, and 150 K temperature mixture and a grain size distribution with a 0.1 μm silicate core radius and an ice mantle extending to as much as 0.6 μm. The 3 μm spectral region in other YSOs could be adequately fitted with other combinations of temperature and maximum mantle radius without implying the presence of NH_3. Smith et al. (1989) also used high-resolution ground-based spectra to estimate upper limits of 1%–2% for the ammonia abundance for both Orion BN and AFGL 989. Whittet et al. (1996) deduced an upper limit of $\sim 8\%$ for ammonia in the infrared source associated with the Herbig-Haro nebula HH 100, and Graham (1998) retracted the earlier Graham & Chen (1991) claim of a 2.97 μm absorption feature in HH 100, HH 54, and HH 57. Dartois & d'Hendecourt (2001) use scattering models to fit the 3 μm spectra of 12 sources and derive upper limits of a few percent up to $\sim 25\%$ for the ammonia abundance in a variety of sources, and discuss possible contributions by ammonium hydrate to the long-wavelength wing of the H_2O feature. Chiar et al. (2000) report NH_3 abundances of 20%–30% relative to H_2O for the Galactic center sources GCS 3I, GCS 4, and Sgr A* based on substructure at the 2.96 μm feature. These three sources are the only ones in our survey that display this obvious feature, although whether or not it is due to the NH stretch of NH_3 is still uncertain.

Recently, solid NH_3 was detected via its 9 μm transition in the massive protostars NGC 7538 IRS 9 and W33 A with abundances of 10% and 15%, respectively (Lacy et al. 1998; Gibb et al. 2000). Hagen, Tielens, & Greenberg (1983) suggested that ammonia abundances of less than $\sim 10\%$ are not discernable in the 3 μm region. Keane et al. (2001) studied the 5–8 μm region and found that the maximum amount of NH_3 that can be present in the ice mantle without changing the 6 μm profile is about 9%, which is marginally consistent with the observations of NGC 7538 IRS 9 and W33 A. With these reports, it is timely to search the *ISO* database for evidence of the 2.96 and 9.0 μm features of ammonia in interstellar ices. We stress the importance of modeling both features as well as checking for consistency at 6 μm, to gain a consistent picture, since there are multiple contributions to each spectral region, which can affect the line profiles. Furthermore, since abundances of up to 10% are difficult to extract from the 3 and 6 μm regions, the 9 μm region can be used to place more stringent limits.

In § 2 we discuss the observations and data reduction procedures used. In § 3.1 we discuss the many contributions to the 8–11 μm profile, while in § 3.2 we discuss the 3 μm H_2O feature and the many factors that can alter its profile. In § 3.3 we review the results of our fitting procedures and derive abundances or upper limits for NH_3.

2. OBSERVATIONS AND DATA REDUCTION

The data used in this research consist primarily of complete grating scans from 2.4 to 45.2 μm in AOT mode S01 (speed 3 or 4) at a resolving power of $\sim R/4$ and $\sim R/2$, respectively (where R, the full grating resolving power of the SWS, ranges from 1000 to 2000). AOT mode S06 scans, which cover limited spectral ranges with the full resolving power of the SWS, were used where available. A detailed description of the SWS and its mode of operation is given by de Graauw et al. (1996). The sources investigated in this study are listed in Table 1. They were chosen by searching the *ISO* SWS database for spectra with S01 speed 3 or higher resolution exhibiting deep ice features of CO_2 and water.

Data reduction was performed at the Space Research Organization of the Netherlands (SRON) in Groningen, The Netherlands, using the standard SWS interactive analysis package and pipeline processing version OLP9.0. A detailed description of the SWS's data reduction procedure can be found in de Graauw et al. (1996). The *ISO* spacecraft records spectra with a grating that scans from low to high wavelengths and then from high to low wavelengths, resulting in two scans (the "up" and "down" scans, respectively). These scans were reduced separately. When flat-fielding, we made a reference flat with the down scan, which is less affected by memory effects, and used this on the up scan. The final up and down spectra were found to agree well in shape and flux level, and the final step was to average the two. In cases of saturated absorption features, as occurs at both 3 and 9 μm in W33 A and AFGL 7009S, we applied a filter to the data. Points with signal-to-noise ratios (S/N) of less than 3 or flux density less than 0.1 Jy were removed (see Gibb et al. 2000 for details). The final spectra are shown in Figures 1 and 2.

We searched the deep 9.7 μm silicate features for the inversion mode of NH_3, which appears as a change in slope at ~ 8.5 μm at the approximate onset of the feature, along with a peak near 9.0 μm. The 3 μm region was also studied for evidence of the N-H stretch feature. We used laboratory data from the Leiden Molecular Astrophysics group[3] and made a least-χ^2 fit to the shape of the 3 μm water feature simultaneously with two laboratory spectra, a warm and a

[3] See http://www.strw.leidenuniv.nl/~lab.

TABLE 1

SUMMARY OF OBSERVATIONS

SOURCE	POSITION (J2000) R.A.	Decl.	AOT	UTC DATE	t_{int} (s)
W3 IRS5	02 25 40.5	62 05 51.3	1.3	1997 Jan 17	3434
AFGL 490	03 27 38.7	58 47 01.1	1.3	1997 Aug 17	3434
Elias 16	04 39 38.8	26 11 26.8	6	1997 Oct 01	8682
Orion BN	05 35 14.2	−05 22 23.6	6	1997 Oct 12	7598
Mon R2 IRS 3	06 07 47.8	−06 22 56.8	1.3	1997 Sep 27	3454
AFGL 989	06 41 10.1	09 29 35.8	1.3	1997 Oct 31	3454
AFGL 2136	11 22 26.2	−13 30 08.3	1.3	1996 Oct 11	3454
Elias 29	16 27 09.3	−24 37 21.1	1.3	1996 Aug 09	3454
SGR A*	17 45 40.0	−29 00 28.6	1.4	1996 Feb 19	6528
GCS 3I	17 46 14.8	−28 49 34.0	1.3	1996 Aug 29	3454
GCS 4	17 46 15.7	−28 49 47.0	1.3	1996 Sep 09	3454
W33 A	18 14 39.4	−17 52 01.4	1.4	1996 Oct 10	6538
AFGL 7009S	18 34 20.6	−05 59 45.2	1.3	1996 Apr 17	3462
AFGL 2591	20 29 24.6	40 11 19.1	1.3	1996 Nov 07	3454
S 140	22 19 18.2	63 18 47.6	1.4	1996 Jun 24	6538
NGC 7538 IRS 1	23 13 45.3	61 28 09.9	1.3	1996 Dec 05	3454
NGC 7538 IRS 9	23 14 01.6	61 27 20.4	6	1996 Feb 23	6894
			6	1997 Dec 06	6264

NOTE.—Units of right ascension are hours, minutes, and seconds, and units of declination are degrees, arcminutes, and arcseconds.

cool component. The laboratory spectra included pure water absorption spectra with temperatures ranging from 10 to 160 K and mixtures of water with 6%, 9%, and 20% ammonia components and temperatures between 10 and 240 K. A complete description of the experimental procedures can be found in Gerakines et al. (1995). We made fits using pure water as well as fits that included both mixtures and pure water. The results of the fitting are discussed in § 3.3. The results for the best fit to the 3 μm feature were then plotted over the 9 μm feature when present to check for consistency. A least-χ^2 fit to the 9 μm feature itself was not performed because of the uncertainty in the continuum and the possibility of contributions to the integrated absorption due to the weak methanol CH_3 rock feature at 8.9 μm, and unidentified excess absorption at 9.2 μm. The latter feature may be intrinsic to the silicate profile itself. In cases where no 9 μm feature is present, upper limits to the abundance were calculated.

3. RESULTS

3.1. *Silicate Spectral Characteristics*

Silicates are ubiquitous, being found in most environments from comets and interplanetary dust particles to dark clouds and embedded YSOs. They form in the circumstellar shells around oxygen-rich post–main-sequence stars and are injected into the interstellar medium via stellar winds. Earlier ground-based spectroscopy of silicates in protostellar regions revealed broad, smooth 10 and 18 μm features indicative of amorphous silicates. Annealed silicate features are found in the envelopes of evolved stars with high mass loss (Waters, Molster, & de Jong 1996), Comet Hale-Bopp (Crovisier et al. 1996), luminous blue variables (Waters et al. 1997), and around isolated objects somewhere between Herbig Ae/Be and β Pic stars in evolution (Waelkens et al. 1996). However, the only evidence for an annealed component in deeply embedded YSOs comes from infrared spectropolarimetry measurements of AFGL 2591 made by Aitken et al. (1988) and Wright et al. (1999). This is consistent with the conclusion of Demyk et al. (1999), who estimate that no more than 1%–2% of silicates in the cold grains (20–40 K) of YSOs AFGL 7009S and IRAS 19110+1045 are annealed. The peak positions of the 10 and 18 μm silicate features are compatible with amorphous pyroxenes containing Fe and some Ca. Laboratory spectroscopy of crystalline silicates show a variety of structures, which are a function of grain size, level of crystallinity, and mineralogy, primarily longward of 10 μm (Brucato et al. 1999; Jäger et al. 1998; Hallenbeck, Nuth, & Daukantas 1998). Bowey & Adamson (2001) report a 9.4 μm feature in ground-based observations of YSOs HL Tau and Elias 7 that is similar in shape to an emission feature in O-rich AGB stars and circumstellar emission found by Monnier, Geballe, & Danchi (1998). They propose that fine structures such as this are carried by crystalline or semicrystalline silicates. Observations of Comet Hale-Bopp also revealed a 9.3 μm feature, which Wooden et al. (1999) attribute to resonances of Mg-rich crystalline or semicrystalline pyroxenes. Annealed crystals of olivine are expected to exhibit a feature at 11.2 μm when present.

Superposed on the silicate feature could be emission at 8.6 and 11.3 μm due to polycyclic aromatic hydrocarbons (PAHs). Several ice mantle constituents also have absorption features in this spectral region, including the C-O stretch (9.7 μm) and the weak C-H_3 rock (8.9 μm) modes of CH_3OH where this molecule is abundant, the 13.3 μm libration mode of H_2O, and the 9.0 μm inversion mode of NH_3. Below we discuss the spectral substructure seen in the 10 μm spectra presented here, and identify absorption due to NH_3 and CH_3OH ices in some of our spectra.

Our *ISO* spectra of YSOs (Fig. 1) also show a 9.2 μm absorption feature (FWHM $\sim$ 0.45 μm) superposed on the silicate band in most cases, although it seems to be very weak or absent in the Galactic center sources GCS 4, GCS 3I, and Sgr A*, as well as in W3 IRS 5 and S140. Of the seven remaining sources, AFGL 2591 has the best S/N in

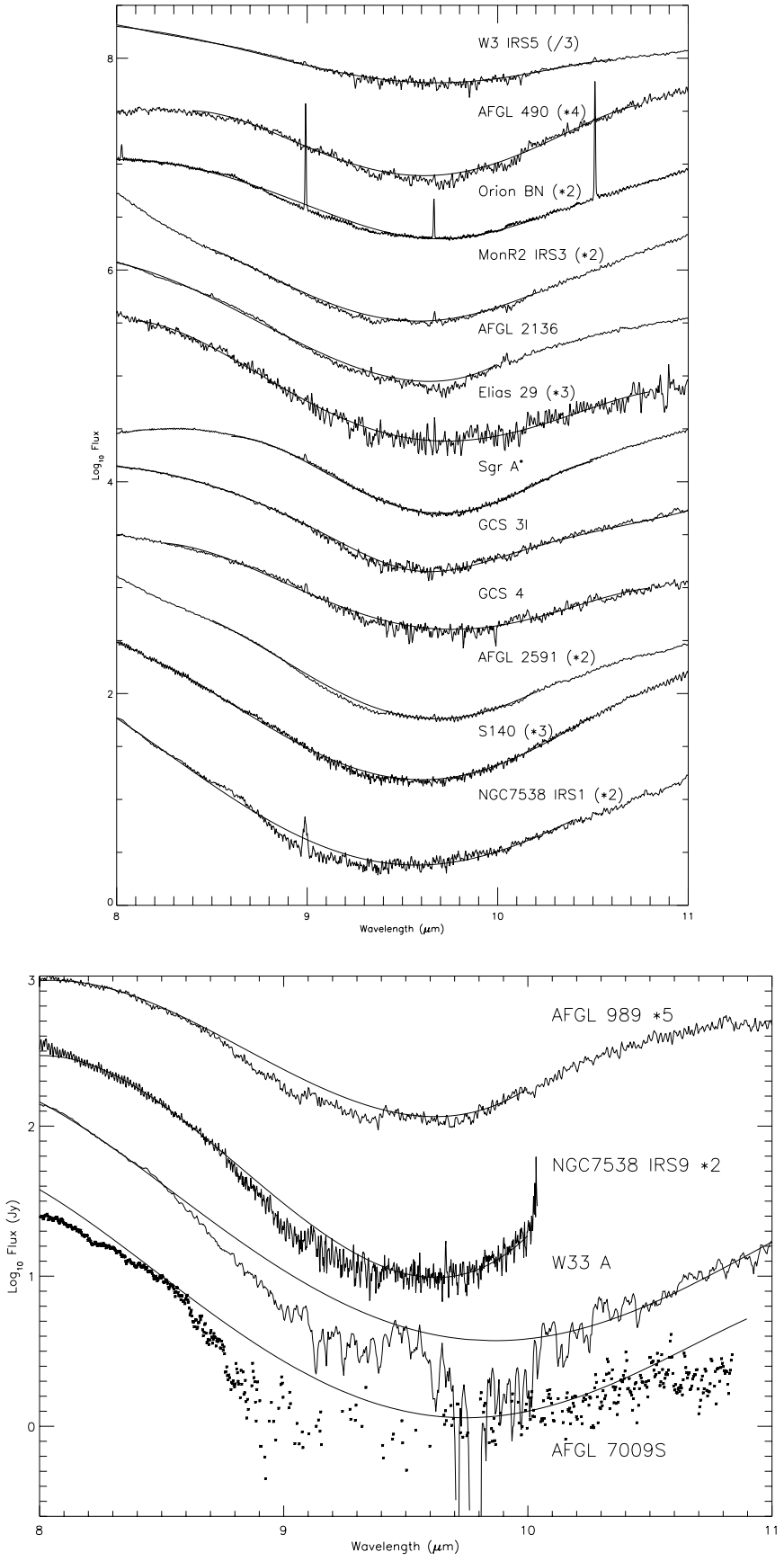

FIG. 1.—Plots of the 8–11 μm spectral region for the 16 sources studied with the continuum fits over plotted. *Top*: Sources for which there is no evidence of NH_3 at 9 μm. *Bottom*: The four sources for which excess absorption, attributed to NH_3, is present at 9 μm. The $\log_{10}$ flux values were shifted up or down when necessary for clarity. Note that the 9.2 μm absorption (and 9.4 μm inflection) is present in most sources except Galactic center source Sgr A*, W3 IRS 5, Elias 29, and S140. This may be due to crystalline or semicrystalline Mg-rich pyroxenes (Wooden et al. 1999).

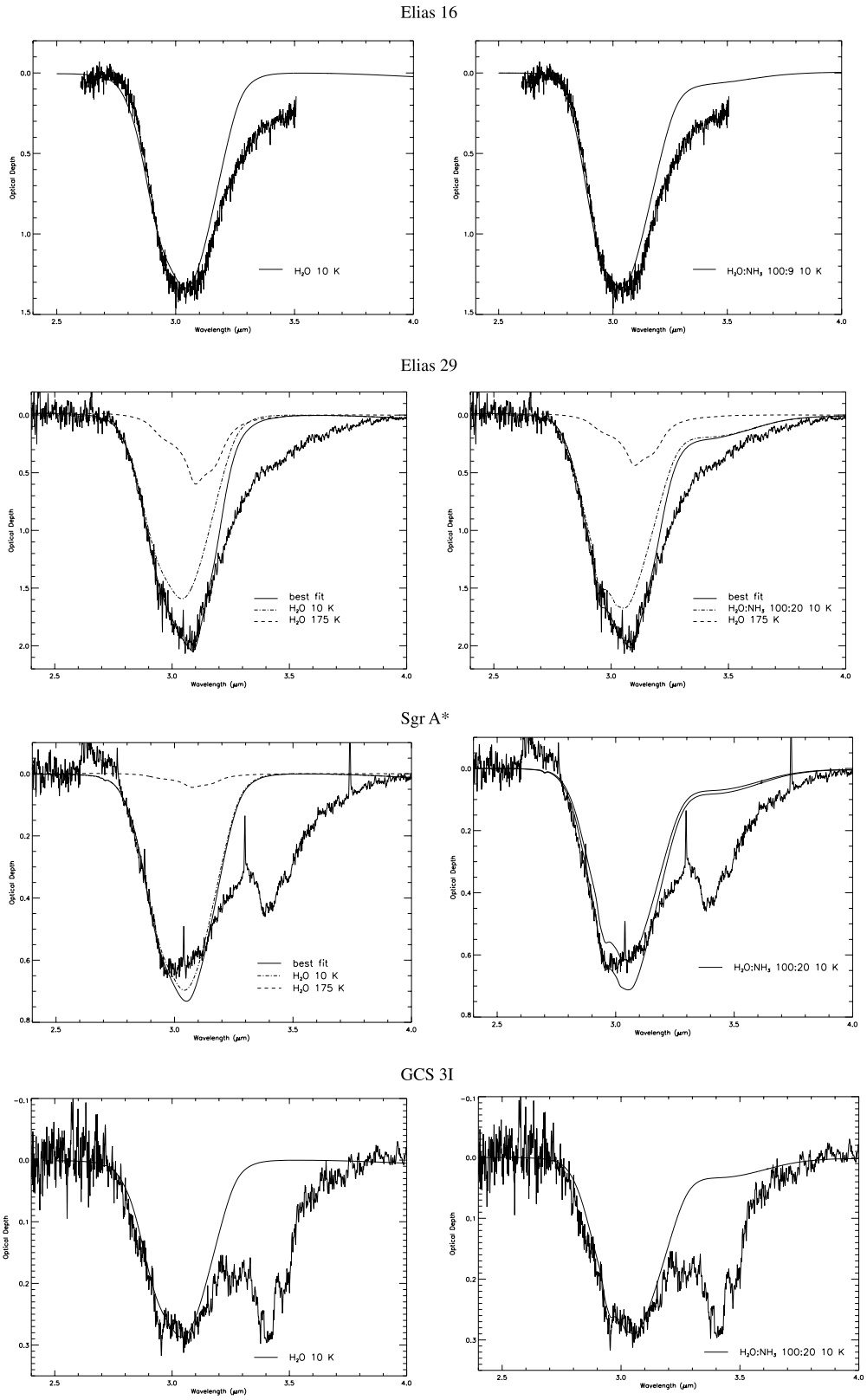

FIG. 2.—Least-χ^2 fits to the 3 μm water profiles of Elias 16, Elias 29, Sgr A*, GCS 3I, GCS 4, Orion BN, AFGL 490, AFGL 989, AFGL 2136, AFGL 2591, S140, NGC 7538 IRS 9, Mon R2 IRS 3, and W3 IRS 5. The dashed line shows the hot component, the dash-dotted line shows the cold component, and the solid line is the sum of the two. The left column shows the best fit for a two-temperature component pure H_2O mixture, and the right column shows the best fit for two temperature components with both pure H_2O and H_2O:NH_3 mixtures available to the fitting routine. Both conditions give comparable fits with similar least-χ^2 values. For results in which a single, cold temperature gave the best result, only a single fit is shown. Note that the fits for Elias 16 indicate that there could be up to 10% NH_3 present in the ice mantle. The W33 A, AFGL 7009S, and NGC 7538 IRS 9 spectra are saturated at 3 μm, and we did not derive fits for these sources.

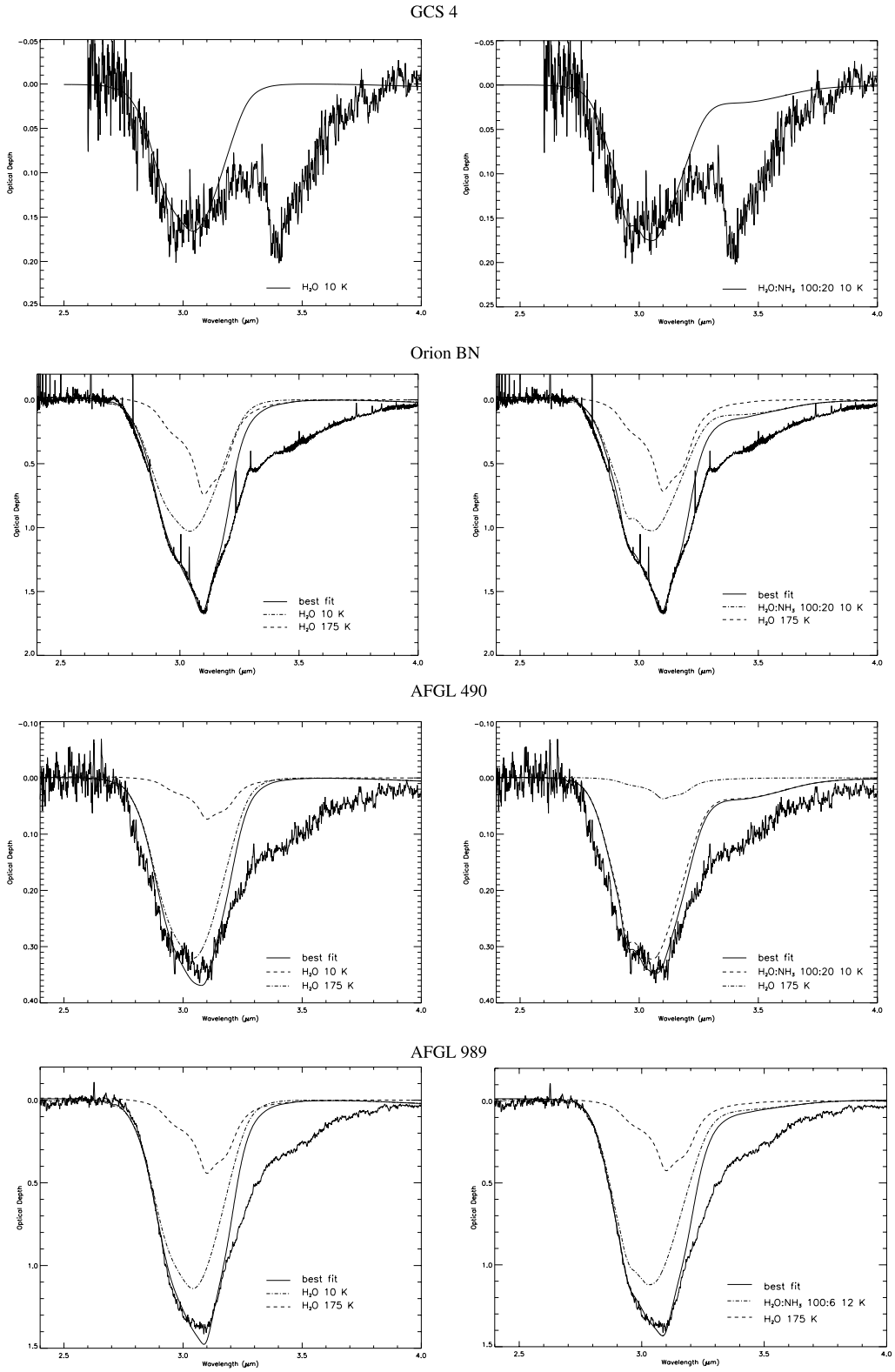

FIG. 2.—*Continued*

this region and is free from emission features that may confuse our continuum placement. Using the fit shown in Figure 1, we derived a reference 9.2 μm feature, which we compare to the excess absorption in our four NH_3-bearing sources discussed below and shown in Figure 4. We note that the width and shape of this feature is consistent to within the scatter for all the sources in which it is present. Mon R2 IRS 3, Orion Irc 2, AFGL 490, Elias 29, and AFGL 989 all have weak excess absorption near 10.1 μm. In addition to this, most sources in this study show a broad tilde-shaped feature between 10.6 and 11.4 μm. While these could be due to structure in the silicate profile, it is also

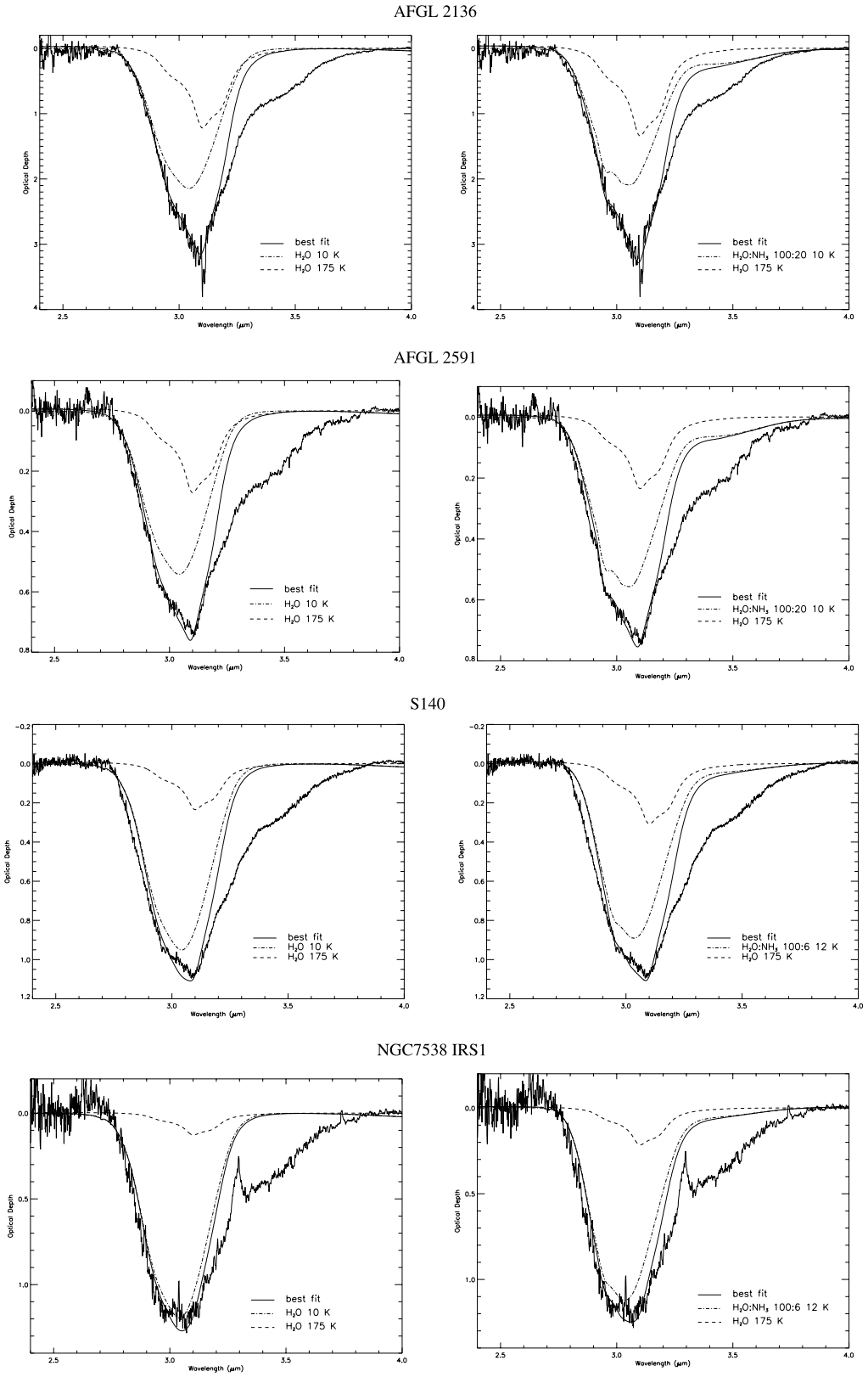

FIG. 2.—*Continued*

possible that these could be due in part to residues from the instrumental spectral response function correction at 10.1 and 11.0 μm. For this reason, these spectral regions were not considered when fitting the continuum.

Only four sources show a distinct change in slope at 8.5 μm with a 9.0 μm absorption peak superposed on the silicate feature that characterize NH_3 ice absorption. They are W33 A, NGC 7538 IRS 9, AFGL 989, and AFGL 7009S. Figure 1 shows several representative silicate features. Figure 1 (*top*) shows the 12 sources for which no excess 9 μm absorption is evident: W3 IRS 5, AFGL 490, Orion BN, Mon R2 IRS 3, AFGL 2136, Elias 29, Sgr A*, GCS 3I, GCS

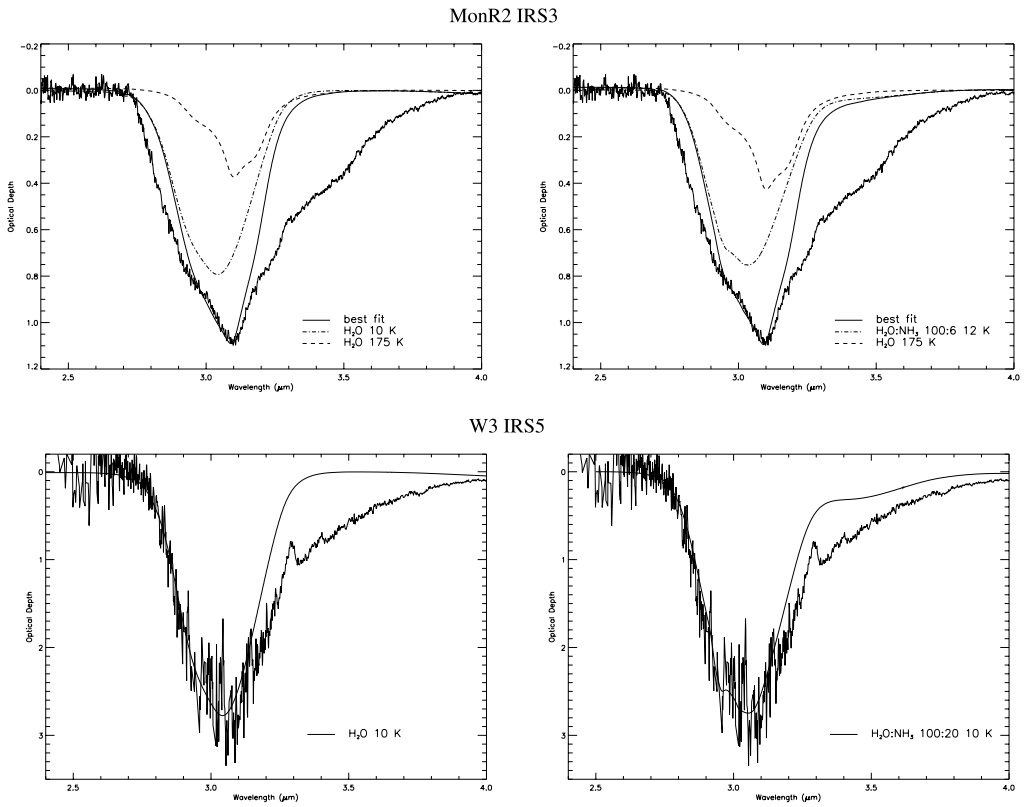

FIG. 2.—*Continued*

4, AFGL 2591, S140, and NGC 7538 IRS 1. Figure 1 (*bottom*) shows the same spectral region for our four candidate NH_3-bearing sources: AFGL 989, NGC 7538 IRS 9, W33 A, and AFGL 7009S, with the chosen continua overplotted. There is no continuum fit for AFGL 7009S, since the feature is saturated at 9 μm and there are few data points left between 9.2 and 9.6 μm to constrain the fit after we impose our filter (see § 2). Instead, we overplotted the continuum fit for W33 A, which is an approximate match, to illustrate the presence of a feature and estimate its optical depth. We have determined that to within the uncertainties, there is no correlation between the tilde-shaped 11 μm feature or the 10.1 μm feature with that at 9.0 μm. However, with the ice and silicate composition both unknown, it is difficult to know where to place a silicate continuum in order to extract possible ice features. We have fitted polynomials to the underlying silicate feature by making 8.3–8.5 μm, the inversion at 9.4 μm, and 10.2–10.6 μm the continuum positions. The resulting optical-depth plots for the four potential ammonia features are discussed in § 3.3.

3.2. *Ammonia at* 3 μm*?*

Many factors influence the shape of the water profile. There is the possibility of superposition of absorption features by other ices occurring in the same spectral range, such as the C-H stretch absorptions between 3.2 and 3.6 μm. Thermal history will also affect the shape of the profile. As the temperature of the water ice increases, the peak of the feature shifts to longer wavelengths and the profile narrows as the amorphous ice is crystallized. This results in what appears to be a wing at 2.96 μm, illustrated in Figure 3, which plots the 3 μm laboratory spectra for water at both 10 and 160 K. Scattering also causes a slight shift to longer wavelengths and a broadening of the feature, as shown by Smith et al. (1989; their Fig. 3). Scattering models have been studied by Smith et al. (1989) and Dartois & d'Hendecourt (2001), and the reader is referred to these papers for more details.

Physically, there are likely to be grain size distributions, temperature distributions, and geometrical effects affecting the 3 μm profile in the lines of sight to the objects in this

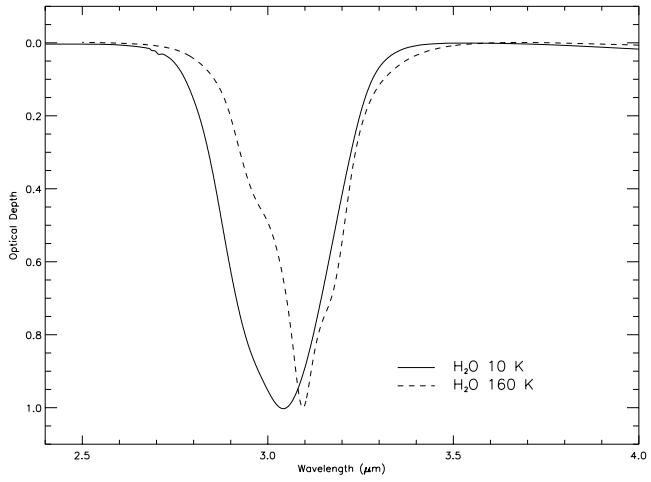

FIG. 3.—Comparison of spectra for pure water at 10 and 160 K from the Leiden database with optical depth normalized to 1. This illustrates that increasing temperature narrows the profile and shifts the peak position to longer wavelengths. Note the "wing" shape at 2.95 μm in the 160 K data.

study, in addition to variations in ice mantle composition and crystallinity (thermal history). Clearly, the question of the abundance of NH_3 ice cannot be answered unambiguously with so many different physical parameters, several of which can provide equally good fits to the short-wavelength side of the 3 μm water feature. Our results illustrate this. In Figure 2 we show optical depth plots for the sources we investigated. Most sources are best fitted by a two-component temperature mixture, although for some sources a single, cold temperature was a better match to the profile. The left column shows the best fit for pure H_2O, and the right column for the H_2O:NH_3 mixtures from the laboratory spectra discussed in § 2. We do not consider scattering, geometry, or more than two temperatures in these fits. Our point is adequately made with a simple least-χ^2 fit directly to the laboratory data. Table 2 gives the ratios of the least-χ^2 values for the best pure water and best water/ammonia laboratory mixtures. With few exceptions, the errors for the two fits are within 13%, which shows that analysis at 2.96 μm alone is not adequate to answer conclusively the question of whether or not NH_3 is present and in what abundances, without a clear understanding of the physical conditions along the line of sight. To do this, we investigate the 9.0 μm feature and check for consistency between the two (see § 3.3).

3.3. *Derived* NH_3 *Abundances*

We investigated the mid-IR spectra of 17 *ISO* sources (see Table 1) for evidence of NH_3 ice. Of these 17 sources, four (including the previously reported detections for NGC 7538 IRS 9 and W33 A) have the change in slope at $\sim$8.5 μm and peak at 9.0 μm that could be attributed to ammonia. For the other 12 sources, no absorption peak is present at 9 μm and only upper limits could be calculated. These abundances and upper limits are reported in Table 2. In addition to these sources, we investigated the 3 μm water feature in Elias 16 to determine an upper limit for the NH_3 abundance.

In cold clouds, ammonia formed by cold gas phase reactions or surface catalysis is expected to stick to the polar ice mantles. This suggests that ammonia should be present toward the background source Elias 16 in the Taurus Molecular Cloud, which is believed to be free from the influence of massive star formation. However, there are no SWS observations of the 9 μm region in this source because of its intrinsic faintness. The 3 μm water feature is shown in Figure 2. The spectrum is dominated by cold ice, with narrow gas-phase OH lines from the background K1 III giant superposed (Elias 1978). The best pure water fit is for 10 K. A good fit is also found using a 10 K mixture of H_2O:NH_3 100:9. It can be seen that the two profiles are very similar. While the presence of ammonia cannot be deduced conclusively, the quality of the data is such that we estimate that an NH_3 abundance of up to 10% relative to H_2O is consistent with the profile, theoretical work (Charnley, Tielens, & Millar 1992), and laboratory studies (Sandford & Allamandola 1993).

Elias 29 is a low-luminosity (36 $L_\odot$) class I protostar in the ρ Oph molecular cloud at a distance of $\sim$160 pc. The water feature is dominated (79% of the total absorption) by a cold ($\sim$10 K) component, but shows evidence of a warm (21%) annealed component as well. The best fit is for a pure water mixture, which gives an excellent fit to the short-wavelength wing of the feature, although an H_2O:NH_3 100:20 at 10 K (86%) and H_2O at 175 K (14%) mixture also gives a reasonable fit. There is a slight excess absorption that peaks at 2.94 μm and is present in both scans. However, the position and profile are not consistent with

TABLE 2

AMMONIA LIMITS FROM SILICATE FEATURE

Source	$N(H_2O)$[a] ($\times 10^{17}$ cm^{-2})	$\chi^2_{H_2O}/\chi^2_{NH_3}$	$\tau_{9.0}$	$N(NH_3)$[b] ($\times 10^{16}$ cm^{-2})	$N(NH_3)/N(H_2O)$ (%)
W3 IRS 5	51	1.13	<0.055	<29	<5.7
AFGL 490	6.2	0.94	<0.02	<10	<17
Elias 16	25	1.05	...	<25[c]	<10[c]
Orion BN	26	1.39	<0.05	<25	<9.5
Mon R2 IRS3	19	0.98	<0.0094	<4.9	<2.6
AFGL 989	24	1.13	0.021 ± 0.007	11 ± 3.2	4.6 ± 1.3
AFGL 2136	51	0.83	<0.021	<11	<2.1
Elias 29	34	0.88	<0.050	<25	<7.4
Sgr A*	12.4	1.28	<0.012	<6.1	<4.9
GCS 3I	4.7	1.05	<0.034	<18	<38
GCS 4	3.0	1.09	<0.030	<16	<53
W33 A	110	...	0.45	170 ± 40	~ 15
AFGL 7009S	110	...	$\sim 0.5 \pm 0.2$?	$\sim 190 \pm 80$?	$\sim 17 \pm 7$?
AFGL 2591	12	1.12	<0.0051	<2.7	<2.2
S140	19	0.97	<0.013	<6.8	<3.6
NGC 7538 IRS 1	22	0.96	<0.071	<37	<17
NGC 7538 IRS 9	70	...	0.20 ± 0.04	105 ± 19	15 ± 3

[a] All values are found using the 3 μm water feature. The values for Sgr A*, GCS 3I, and GCS 4 are from Chiar et al. 2000. The W33 A value is from Gibb et al. 2000. That for AFGL 7009S is from Keane et al. 2001, based on the 6 μm feature, since nearly the entire 3 μm profile is saturated. The rest of the H_2O column densities are from integrating over the best laboratory fit as discussed in § 3.2 and are consistent with the values found in Keane et al. 2001.

[b] Upper limits derived using $A = 1.3 \times 10^{-17}$ cm per molecule (Kerkhof, Schutte, & Ehrenfreund 1999) and a FWHM of 68 found from the H_2O:NH_3 laboratory mixtures from the Leiden Molecular Astrophysics Group database.

[c] Estimated from a laboratory fit to the 3 μm feature (Fig. 2).

NH_3. There is also no evidence for a feature at 9 μm, and we derive an upper limit of 7.4%.

Sgr A* is a Galactic center (GC) source suffering $\sim$30 mag of visual extinction (Lutz et al. 1996). The SWS aperture was centered on the infrared source IRS 7 and contains H II regions, M giants, and supergiants. The GCS 3 and GCS 4 regions are located 40 pc from the Galactic center and make up the infrared quintuplet. GCS 3 has contributions from four separate sources, while GCS 4 is alone in the SWS beam (Schutte et al. 1998). Chiar et al. (2000) reported NH_3 abundances of 20%–30%, that of water based on the prominent substructure at 2.96 μm for Sgr A*. The GCS 3 and GCS 4 profiles were also found to be consistent with the laboratory data used to fit Sgr A*, implying 20%–30% abundances of NH_3 toward the Galactic center. The low water-ice column densities and hence low ammonia column densities make detection of the 9.0 μm NH_3 feature impossible in the *ISO* observations of GCS 3 and GCS 4 for which we have derived upper limits of 38% and 53%, respectively. However, the higher water column density and S/N in the silicate feature would suggest that NH_3 should be detectable in Sgr A*. Indeed, a 20%–30% ammonia abundance should give a feature with an optical depth of $\sim$0.05–0.07, which is well outside the error bars for that region. There is no feature in evidence, and it seems unlikely that the lack of structure at 9 μm could be due to the addition of several species of ice and silicates that serve to smooth out the profile. However, this possibility cannot currently be ruled out, since the contributions to the silicate feature from the multiple sources are not well characterized, and it is known that there are sources with both silicate emission and absorption in the beam. Our upper limit places the abundance at less than 5% that of water, although we caution that further observations of individual sources within the SWS beam are required for a complete treatment of this line of sight. In the 2–4 μm spectral region, there are emission features due to H I at 2.626, 2.758, 2.873, 3.039, 3.297, and 3.740 μm. For this reason, we used the spectral region shortward of 2.6 μm as continuum. We note that the 3 μm profile in Sgr A* is unique in that it peaks at 2.96 μm. The other sources in this study peak longward of 3 μm, with a few that have a narrow peak at 2.96 μm, which is not firmly identified (i.e., NGC 7538 IRS 1, AFGL 490, GCS 3I). An ammonia mixture can only account for this stronger absorption at 2.96 μm if the concentration of NH_3 is about 30% or higher. However, the long-wavelength shoulder due to ammonium hydrate for concentrations this high begins to overestimate the optical depth longward of 3.5 μm. In Figure 2 we show two possible fits for a 20% ammonia mixture. If we fit the short-wavelength wing, the peak optical depth is obviously overestimated. However, if we scale the laboratory data to fit the optical depth, the rest of the spectrum is a poor match. The excess absorption at 2.96 μm might be due to the superposition of spectral features from the many infrared sources within the $14'' \times 20''$ *ISO* SWS beam, or to scattering effects, rather than ammonia. The other two Galactic center sources do not have this problem and are fitted equally well with cold pure water or a cold 20% ammonia mixture. Further investigation is required to satisfactorily answer the question of the nature of the Sgr A* 3 μm profile.

BN is a luminous infrared source ($L \sim 2500\ L_\odot$) in the Orion Molecular Cloud complex, 450 pc away, probably illuminated by a B3–B4 star, with many other infrared sources also in the SWS beam (Gezari, Backman, & Werner 1998). Its infrared spectrum is very similar to that of Orion Irc 2 (which is also within the SWS beam) and is rich in ice absorption as well as PAH and ionized metal emission features from the foreground photodissociation region (PDR) and H II region (van Dishoeck et al. 1998). The 3 μm water feature has a very narrow peak at 3.1 μm, indicative of a warm, annealed water-ice component. There is also a very prominent wing at 2.96 μm, which has been interpreted to be due to either the presence of ammonia (Knacke et al. 1982) or scattering by large grains (Smith et al. 1989; Pendleton, Tielens, & Werner 1990). Our least-χ^2 fits to this spectrum (see Fig. 2) show reasonable results for pure water with a $\sim$10 K (67% of the total absorption) and $\sim$175 K (33%) component. This is consistent with the 23:77:150 K = 5.3:2.5:1 best-fit mixture found by Smith et al. (1989). The fit is improved slightly by replacing the pure cold water with a H_2O:NH_3 100:20 mixture at 10 K. The 9.7 μm silicate feature in BN shows an abrupt change in slope at $\sim$8.5 μm; however, this may be due to the presence of a weak PAH emission feature at 8.6 μm. There is also a very strong Ar III emission line at 9.0 μm, where the ammonia feature is expected to peak. The PAH emissions make it difficult to fit a reliable continuum and hence to extract any possible absorption feature. The best fit for the 3 μm feature results in a feature of optical depth $\sim$0.07 in the silicate feature, which corresponds to the level of the error bars for that region of the spectrum. The maximum acceptable abundance based on the continuum fit in Figure 1 (*top*), interpolating across the Ar III emission feature, is $\sim$9.5%.

AFGL 490 is a young, isolated, intermediate-luminosity (2200 $L_\odot$; Mozurkewich, Schwartz, & Smith 1986) star-forming region hidden by 17–50 mag of visual extinction (Rieke & Lebofsky 1985) located about 1 kpc away (Snell et al. 1984). This source has one of the lowest water column densities of the objects included in this study (see Table 2). The water feature is best fitted by a mixture dominated by cold ice (86%, 10 K) with a small (14%) warm (175 K) component. There is excess absorption at 2.96 μm, which can be fitted with a H_2O:NH_3 100:20 mixture (93%) and a small (7%) H_2O (175 K) component, although the difference in the errors for the pure water and mixture fits are only 6%. The 9 μm profile exhibits the structure at 9.2 μm that is present in most of our spectra, but there is no evidence of NH_3. An upper limit of 17% was determined.

AFGL 989 is an intermediate-mass young stellar object embedded in a dense cloud core in the NGC 2264 cloud complex near the apex of the Cone Nebula 800 pc away and surrounded by embedded low-mass stars (Schreyer et al. 1997). This source lies behind 20–30 mag of extinction (Thompson et al. 1998). AFGL 989 exhibits a very high abundance of N_2H^+ and presumably N_2 in the gas phase. However, Schreyer et al. (1997) report an abundance of 1.2×10^{-8} that of H_2 for NH_3, which is not abnormally high for such an object. Figure 2 shows the best fits to the 3 μm region. The best fit for pure water indicates a cool 10 K (79%) and hot 175 K (21%) component. A slightly improved fit to the low-wavelength profile is achieved using a 12 K H_2O:NH_3 100:6 mixture (80%) with a smaller (20%) 175 K component. A higher NH_3 concentration than this can be ruled out, since it would not be compatible with the profile. The silicate feature in this source has a change in slope at 8.5 μm, the approximate cut-on for a polar ammonia mixture. There are weak absorption features at

9.0, 9.2, and 9.75 μm, which could be due to NH_3, silicate structure, and CH_3OH, respectively (see Fig. 1). There is no frozen methanol abundance in the literature for this source, and there is no evidence of the C-H stretch feature at 3.54 μm, so we did not include that in the plot. We note, however, that the 9.0 and 9.75 μm regions are consistent with a small methanol abundance of less than 5%. The abundance, found from the best fit to 3 μm, is consistent with the strength of the 9.0 μm feature, as shown in Figure 2. The best-fit ammonia mixture is overplotted on the 9 μm region in Figure 4. The right column shows the residual left after subtracting the best fit from the optical-depth plot. The thick line is the 9.2 μm feature from AFGL 2591, scaled in optical depth to fit the residual. We determined a total column density of $11 \pm 3 \times 10^{16}$ cm^{-2} for ammonia.

AFGL 2136 is a very hot, 7×10^4 $L_\odot$ source 2 kpc away, with temperatures along most of the line of sight of $\approx$30 K or more, as inferred by the low abundances of apolar ice species (Sandford et al. 1988; Schutte et al. 1996) and by modeling submillimeter flux densities (van der Tak et al. 1999). The best fit for AFGL 2136 is for pure water composed of a 10 K and a substantial ($\sim$30% of the total absorption) warm, annealed component, although a H_2O:NH_3 100:20 mixture for the cold ice component is within the errors of the 3 μm profile. If the dust is warm, NH_3 would be expected to have sublimated along much of the line of sight, so a nondetection for this source is not entirely unexpected. We note that there is little difference between 10 and 30 K laboratory profiles, so our best fit is consistent with a substantial component of the grains having a temperature of about 30 K. The silicate feature is not compatible with an abundance of more than about 2%.

AFGL 2591 is an apparently isolated luminous (2×10^4 $L_\odot$) YSO 1 kpc away, obscured by 70 mag of visual extinction (Carr et al. 1995). Aitken et al. (1988) reported a detection of an 11.2 μm polarization feature, which they interpreted to be evidence for an annealed silicate grain component in this source. There is no evidence for structure at 9.0 μm or a change in slope near 8.5 μm, and the excellent S/N allows an upper limit of 2.2% relative to water. This is a far more stringent limit than indicated by the 3 μm fit (Fig. 2), where a H_2O:NH_3 100:20 (10 K, 79%) and H_2O 175 K (21%) mixture gives the best fit. Reasonable results are also achieved with a pure water 10 K (74%) and 175 K (26%) fit. The lack of excess emission or absorption structure in the silicate profile of this source, with the exception of the 9.2 μm feature, coupled with the good S/N, make this source the template for the 9.2 μm absorption feature (see the discussion in § 3.1).

S140 is an H II region 0.9 kpc away that is currently undergoing both high- and low-mass star formation (van der Tak et al. 1999). Gas-phase ammonia maps have been made of this region, and a kinetic temperature decreasing from 40 to 20 K and a column density for NH_3 of $\sim 10^{15}$ cm^{-2} have been derived (Ungerechts, Walmsley, & Winnewisser 1986). There is no evidence of ammonia superposed on the silicate feature. The 3 μm region is fitted equally well by either a pure water 10 K (85%) and 175 K (15%) mixture or a H_2O:NH_3 100:6 12 K (80%)/H_2O 175 K (20%) mixture. A calculation using the 5%–10% abundance limits of ammonia allowed by fits to the 3 μm feature would give a 9 μm feature with an optical depth of $\sim$0.02–0.03, slightly over the error limits ($\sim$0.01). The upper limit derived from the silicate feature is 3.6%.

NGC 7538 IRS 1 appears to be the youngest and most luminous (1.3×10^5 $L_\odot$) pre–main-sequence object in the H II regions and molecular clouds that make up the NGC 7538 complex (Strazzulla et al. 1998). It is located 2.8 kpc away in the Perseus arm and, like Orion BN, also has a rich spectrum with PAH and metal ion emission from the presence of an H II region in the SWS aperture superposed on the absorption profile. Both pure H_2O at 10 K (93%) and 175 K (7%) and H_2O:NH_3 100:6 at 12 K (88%) with a small (12%) 175 K H_2O component give good fits to the 3 μm feature. The 8.6 μm PAH and the 8.99 μm Ar III emission features make it impossible to reliably detect any possible ammonia feature. We place an upper limit at 17%. The 2.98 μm substructure is inconsistent with NH_3 in both position and width.

NGC 7538 IRS 9 ground-based observations by Lacy et al. (1998) resulted in the first detection of the 9 μm NH_3 feature. They report an abundance of $\sim$10% relative to H_2O. We included this source in our investigation, since there is a higher resolution AOT06 observation of this source in the SWS archive. We also find a feature at 9 μm with the same optical depth ($\sim$0.35) as reported by Lacy et al. (1998). However, Lacy et al. (1998) used a water abundance based on the 6 μm feature. As has been shown in several other sources (Gibb et al. 2000; Chiar et al. 2000), this often results in an overestimate of the water column density by a factor of 2 or more. This is the case in this source as well. Keane et al. (2001) report a column density of 7×10^{18} cm^{-2} based on the 3 μm feature, while the 6 μm feature indicates a column density of 10×10^{18} cm^{-2}. A CH_3OH column density of 9.1×10^{17} cm^{-2}, consistent with the $\sim 1.2 \times 10^{18}$ cm^{-2} that we find using the 3.54 μm feature in the SWS data, has been reported (Allamandola et al. 1992), which gives a feature of $\tau \sim 0.035$ at 8.9 μm, shown by the dashed line in Figure 4. The excess absorption at 9–9.4 μm is likely due to silicates, as discussed in § 3.1; hence, we fit the ammonia and methanol ice features to the short-wavelength side (8.5–9 μm). Subtracting the contribution due to CH_3OH, we find an NH_3 column density of 1.0×10^{18} cm^{-2}, which gives an abundance $\approx$15% that of H_2O using the 3 μm column density, or $\approx$10% when using the 6 μm column density. This is consistent with the results of Keane et al. (2001), who find that an abundance of up to 10% is permitted without altering the 6 μm profile. After subtracting the best fit from the optical depth plot, we plot the 9.2 μm silicate profile from AFGL 2591, which does not show any evidence of a feature at 9.0 μm and has good S/N, over the residual, and find good agreement, providing support that we have accounted for all the ice absorption at 9 μm.

The molecular cloud core containing Mon R2 IRS 3 is a vigorous star-forming region about 1 kpc away that shows evidence of a molecular outflow and circumstellar disk, which could explain why it is one of the brightest thermal infrared sources in the Galaxy (Koresko et al. 1993). It may consist of a dense cluster of young stars rather than a single luminous one (Persi et al. 1996). It has a very broad 3 μm water feature that peaks at 3.1 μm and shows structure indicating a very warm, annealed component to the ices, including a shoulder at 2.96 μm. None of the mixtures do well at matching the low-wavelength wing, including those with an ammonia component. Both fits are composed primarily of cold (10 K H_2O or 12 K H_2O:NH_3 100:6, 75%) with $\approx$25% of the absorption due to the 175 K H_2O com-

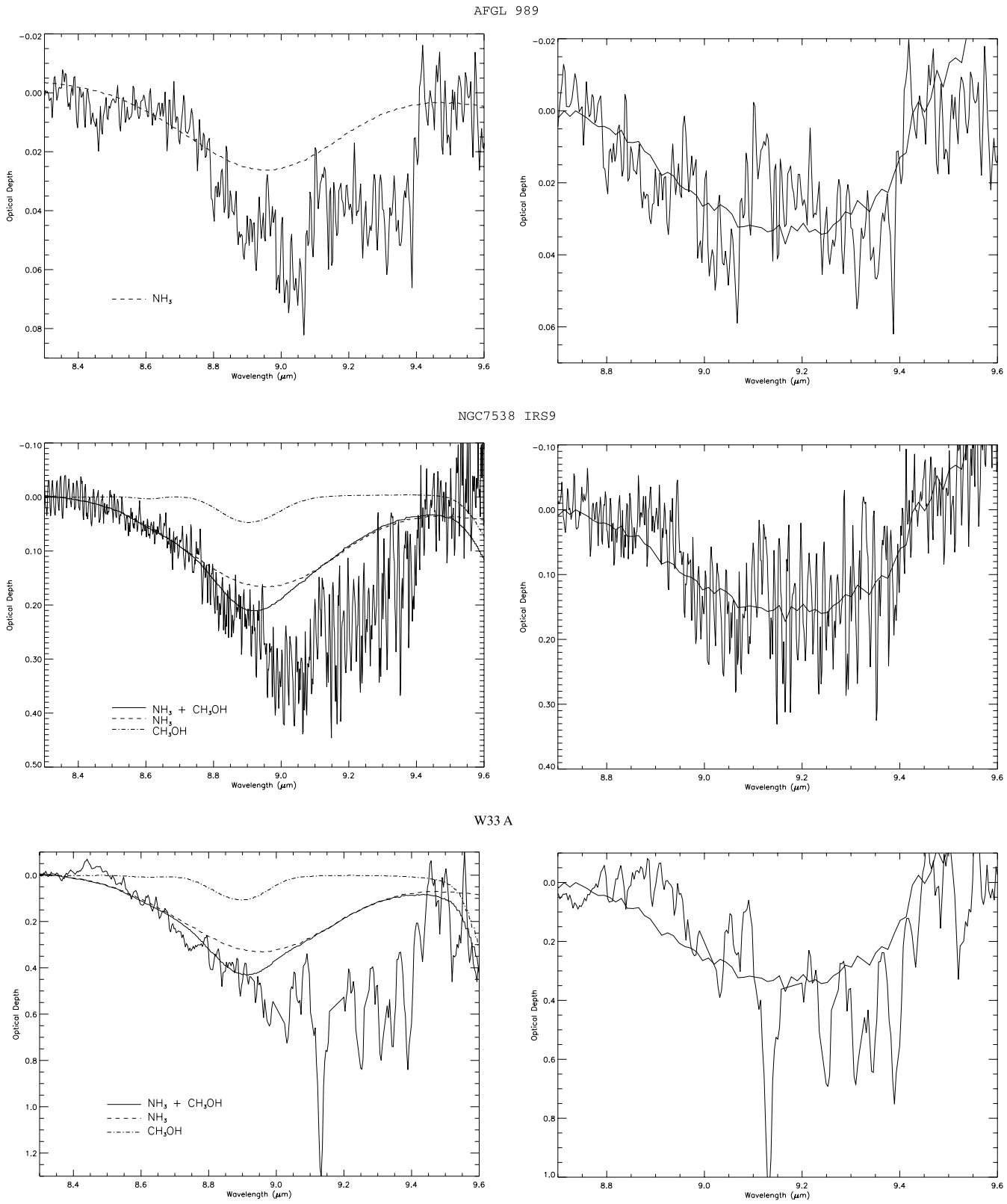

FIG. 4.—Plot of the three sources for which a distinct 9.0 μm absorption feature is present. Overplotted on these are the best-fit H_2O:NH_3 mixture to the 3 μm feature (*dashed line*; 9% NH_3 for W33 A and NGC 7538 IRS 9, and 6% for AFGL 989) and the contribution due to CH_3OH (*dash-dotted line*). We then subtracted this from the total optical depth (*right column*) and overplotted the 9.2 μm feature (*thick line*) from AFGL 2591, smoothed to a resolution of 750 and scaled to match the optical depth of the residual.

ponent. Smith et al. (1989) fitted MRN scattering models (Mathis et al. 1977) to this source and found that the core of the feature was well fitted with an 80 K annealed laboratory fit and that a cold (23 K) component contributes to the short-wavelength wing but still does not result in an adequate fit. The silicate feature has good S/N in the 8–9.2 μm region, and we determine an upper limit for NH_3 of 2.6%.

The W3 Giant Molecular Cloud is a complex of H II regions and molecular cloud material in the Perseus arm 2.3 kpc away (Georgelin & Georgelin 1976). Ongoing star formation is evidenced by OH and H_2O masers as well as outflows. The source IRS 5 is an ultracompact H II region that is double-peaked in the infrared. This source is probably a compact OB association (Claussen et al. 1994). The 3 μm feature is deep and the central wavelength region has a low S/N, giving little constraint on an ammonia column density. The best fit is for a H_2O:NH_3 100:20 10 K mixture, although the fit for pure H_2O at 10 K is comparable. There is also no indication of a feature at 9 μm, and we are able to place an upper limit of about 6%.

W33 A is a massive, luminous (1.1×10^5 $L_\odot$) YSO located $\sim$4 kpc away in the W33 H II molecular cloud complex. Detection of NH_3 via the 9 μm feature was reported by Gibb et al. (2000) with an abundance of $\sim$15% that of water, based on the water column density derived from the 3 μm feature. Figure 1 shows the silicate spectral region for W33 A with the continuum fit overplotted, exhibiting evidence of a 9 μm absorption feature. This is consistent with the constraints imposed by the 6 μm water feature as well (Keane et al. 2001). The reader is referred to Gibb et al. (2000) for more details.

AFGL 7009S is a 3×10^4 $L_\odot$ ultracompact H II region located at 3 kpc (van der Tak et al. 2000). It is classified as a class I late O or early B type star with an ice mantle along the line of sight dominated by cold (21 K) temperatures (Dartois, Gerin, & d'Hendecourt 2000). We do not attempt to fit the silicate profile here because of its saturation at 9–10 μm, which is more extreme than that of W33 A. The 3 μm profile is saturated as well. We note, however, that this source also has the characteristic change in slope at $\sim$8.5 μm and excess absorption at 9 μm that could be attributable to NH_3 absorption with an optical depth of up to $\sim$0.5 when a possible contribution from 9.2 μm (similar to that for W33 A) is taken into account. Figure 5 shows the optical depth plot of AFGL 7009S after the 9.2 μm feature fitted to W33 A has been subtracted out. Overplotted is an H_2O:NH_3 100:9 10 K mixture with an optical depth of $\sim$0.5, to illustrate the presence of a 9 μm feature in this source, along with the contribution due to methanol (Dartois et al. 1999). Further observations are needed to fully characterize the 9 μm NH_3 feature.

4. DISCUSSION

A main conclusion of this study is that while abundances of 5%–10% are allowable in most sources when fitting laboratory spectra to both 3 and 6 μm spectral regions, the 9 μm region appears to put much stronger restrictions on NH_3 abundances for many sources (see Table 2). Limits of $<$5% were derived for Sgr A*, AFGL 989, AFGL 2136, AFGL 2591, S140, and Mon R2 IRS 3. While some sources, such as Elias 29 and AFGL 2136, show evidence of a substantial warm ($\gtrsim$30 K) temperature component along the

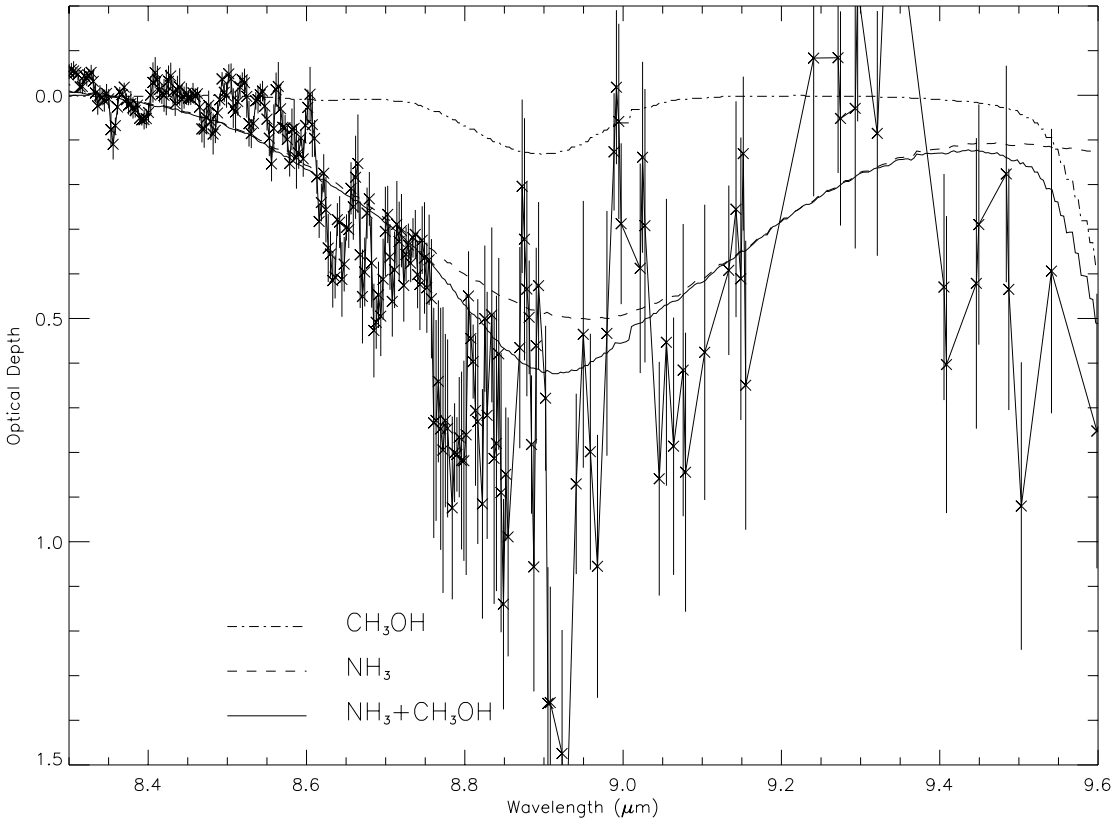

FIG. 5.—Optical-depth plot of the 9 μm feature in AFGL 7009S after a contribution from the 9.2 μm feature (scaled as for W33 A) has been subtracted. Also shown is the contribution due to CH_3OH (*dot-dashed line*) and NH_3 (*dashed line*).

line of sight, other sources, like S140, W3 IRS 5, W33 A, and AFGL 989, show evidence of a substantial cold (~ 10 K) ice component. Ammonia is expected to condense onto icy grain mantles with almost 100% efficiency in the low temperatures found along most of the lines of sight in this study. This is obviously not the case, however, since many cold, dense molecular clouds show substantial abundances of ammonia still in the gas phase, and NH_3 ice seems to be present only in low concentrations, if at all, along most lines of sight. Perhaps this is due in part to nonthermal desorption methods, which have not been accounted for in theories and models. More work needs to be done to solve this mystery.

As discussed in Pendleton et al. (1999), there are two ways of forming the carrier of XCN in the laboratory: UV photolysis of ice mixtures containing NH_3 and ion irradiation of mixtures containing either NH_3 or N_2 (see also Whittet et al. 2001). Therefore, constraining the NH_3 abundance in interstellar ices is important for better understanding how XCN is formed. The proposed formation routes produce different products with different warm-up behaviors. Some products are refractory and survive being heated to room temperature, and others are volatiles that evaporate upon warm-up (Grim & Greenberg 1987; Palumbo et al. 2000). One would expect that if XCN derives from an NH_3-containing ice, there would be an inverse correlation between the abundance of NH_3 and XCN. This is not indicated by our results. W33 A, AFGL 7009S, NGC 7538 IRS 9, and AFGL 2136 all have XCN features and form a set that includes both high ($\sim$10%–15%) and low ($<$2.1%) NH_3 abundances. The experiments of Demyk et al. (1999) indicate that OCN^- is a good candidate for the 4.62 μm feature. This reaction also produces NH_4^+ to conserve charge, which could contribute to the 6.8 μm feature seen in many lines of sight (W. A. Schutte et al., in preparation; Hudson & Moore 2000), suggesting another possible correlation. However, Keane et al. (2001) point out that there does not seem to be a correlation of the 4.62 μm XCN feature with the 6.85 μm absorption, and NH_4^+ does not seem to give a satisfactory fit to the 6.85 μm feature. Further work needs to be done to determine the carrier(s) of the 6.85 μm feature and to determine any possible correlations with the solid NH_3 absorption.

Perturbation of ammonia molecules by water ice results in a very broad excess absorption wing between ~ 3.1 and 3.8 μm, which Dartois & d'Hendecourt (2001) suggested could account for the 3.47 μm absorption feature discovered by Allamandola et al. (1992) and characterized by Brooke et al. (1996, 1999) and Chiar, Adamson, & Whittet (1996) in over a dozen YSOs. We note that the 3.47 μm feature is a relatively narrow (FWHM $\sim$ 0.105 μm) feature between 3.4 and 3.6 μm, which could be due to the stretching vibration of sp^3 C—H bonds but is certainly much narrower than the excess wing due to ammonia interactions with water, which extends from about 3.2 to 3.8 μm. In addition, as pointed out by Smith et al. (1989) and shown in our Figure 2, the ammonium hydrate feature is insufficient to account for most of the excess absorption in the long-wavelength wing. To fit that region with ammonia would require abundances much higher than allowable by the 2.96, 6.16, and 9.0 μm regions. Hence, it is unlikely that anything definitive can be said about the presence of NH_3 by looking solely at this feature.

We conclude that, because of the large number of uncertain parameters (grain shape, grain size distribution, temperature distribution, and mantle composition along the line of sight), the 2.4–4 μm region is insufficient for determining abundances of NH_3 in ice mantles. Upper limits can be derived, however, and multiple spectral regions can be used to assemble a more complete picture of mantle composition and temperature. Extraction of the elusive 9 μm feature from the silicate profile appears to be the surest way to constrain the NH_3 abundance.

E. L. G. and D. C. B. W. gratefully acknowledge financial support from NASA under grants NAG5-7598 and NAG5-9148. J. E. C. is supported by NASA's Long Term Space Astrophysics Program under grant 399-20-61-02. The data presented were analyzed with the support of the Dutch *ISO* Data Analysis Centre (DIDAC) at the Space Research Organization Netherlands (SRON) in Groningen, the Netherlands.

REFERENCES

Aitken, D. K., Roche, P. F., Smith, C. H., James, S. D., & Hough, J. H. 1988, MNRAS, 230, 629
Allamandola, L. J., Sandford, S. A., Tielens, A. G. G. M., & Herbst, T. M. 1992, ApJ, 399, 134
Bernstein, M. P., Sandford, S. A., Allamandola, L. J., Chang, S., & Scharbert, M. A. 1995, ApJ, 454, 327
Blake, G. A., Sutton, E. C., Masson, C. R., & Phillips, T. G. 1987, ApJ, 315, 621
Bowey, J. E., & Adamson, A. J. 2001, MNRAS, 320, 131
Brooke, T. Y., Sellgren, K., & Geballe, T. R. 1999, ApJ, 517, 883
Brooke, T. Y., Sellgren, K., & Smith, R. G. 1996, ApJ, 459, 209
Brucato, J. R., Colangeli, V. M., Palumbo, P., & Bussoletti, E. 1999, A&A, 348, 1012
Carr, J. S., Evans, N. J., Lacy, J. H., & Zhou, S. 1995, ApJ, 450, 667
Cesaroni, R., Churchwell, E., Hofner, P., Walmsley, C. M., & Kurtz, S. 1994, A&A, 288, 903
Charnley, S. B., Tielens, A. G. G. M., & Millar, T. J. 1992, ApJ, 399, L71
Chiar, J. E., Adamson, A. J., & Whittet, D. C. B. 1996, ApJ, 472, 665
Chiar, J. E., Tielens, A. G. G. M., Whittet, D. C. B., Schutte, W. A., Boogert, A. C. A., Lutz, D., van Dishoeck, E. F., & Bernstein, M. P. 2000, ApJ, 537, 749
Claussen, M. J., Gaume, R. A., Johnston, K. J., & Wilson, T. L. 1994, ApJ, 424, L41
Crovisier, J., et al. 1996, A&A, 315, L385
Dartois, E., & d'Hendecourt, L. 2001, A&A, 365, 144
Dartois, E., Gerin, M., & d'Hendecourt, L. 2000, A&A, 361, 1095
Dartois, E., Schutte, W., Geballe, T. R., Demyk, K., Ehrenfreund, P., & d'Hendecourt, L. 1999, A&A, 342, L32
de Graauw, Th., et al. 1996, A&A, 315, L49
Demyk, K., Jones, A. P., Dartois, E., Cox, P., & d'Hendecourt, L. 1999, A&A, 349, 267
Elias, J. H. 1978, ApJ, 224, 857
Elsila, J., Allamandola, L. J., & Sandford, S. A. 1997, ApJ, 479, 818
Federman, S. R., Huntress, W. T., Jr., & Prasad, S. S. 1990, ApJ, 354, 504
Georgelin, Y. M., & Georgelin, Y. P. 1976, A&A, 49, 57
Gerakines, P. A., Schutte, W. A., Greenbert, J. M., & van Dishoeck, E. F. 1995, A&A, 296, 810
Gezari, D. Y., Backman, D. E., & Werner, M. W. 1998, ApJ, 509, 283
Gibb, E. L., et al. 2000, ApJ, 536, 347
Graham, J. A. 1998, ApJ, 492, 213
Graham, J. A., & Chen, W. P. 1991, AJ, 102, 1405
Grim, R. J. A., & Greenberg, J. M. 1987, ApJ, 321, L91
Hagen, W., Tielens, A. G. G. M., & Greenberg, J. M. 1983, A&AS, 51, 389
Hallenbeck, S. L., Nuth, J. A., & Daukantas, P. L. 1998, Icarus, 131, 198
Heaton, B. D., Little, L. T., & Bishop, I. S. 1989, A&A, 213, 148
Hudson, R. L., & Moore, M. H. 2000, A&A, 357, 787
Jäger, C., Molster, F. J., Dorschner, J., Henning, Th., Mutschke, H., & Waters, L. B. F. M. 1998, A&A, 339, 904
Keane, J. V., Tielens, A. G. G. M., Boogert, A. C. A., Schutte, W. A., & Whittet, D. C. B. 2001, A&A, in press
Kerkhof, O., Schutte, W. A., & Ehrenfreund, P. 1999, A&A, 346, 990
Knacke, R. F., & McCorkle, S. 1987, AJ, 94, 972
Knacke, R. F., McCorkle, S., Puetter, R. C., Erickson, E. F., & Krätschmer, W. 1982, ApJ, 260, 141
Koresko, C. D., Beckwith, S., Ghez, A. M., Matthews, K., Herbst, T. M., & Smith, D. A. 1993, AJ, 105, 1481

Lacy, J. H., Farah, H., Sandford, S. A., & Allamandola, L. J. 1998, ApJ, 501, L105
Le Bourlot, J. 1991, A&A, 242, 235
Lutz, D., et al. 1996, A&A, 315, L269
Marquette, J. B., Rowe, B. R., Dupeyrat, G., & Roueff, E. 1985, A&A, 147, 115
Mathis, J. S., Rumpl, W., & Nordsieck, K. H. 1977, ApJ, 217, 425
Monnier, J. D., Geballe, T. R., & Danchi, W. C. 1998, ApJ, 502, 833
Mozurkewich, D., Schwartz, P. R., & Smith, H. A. 1986, ApJ, 311, 371
Palumbo, M. E., Strazzulla, G., Pendleton, T. J., & Tielens, A. G. G. M. 2000, ApJ, 534, 801
Pendleton, Y. J., Tielens, A. G. G. M., Tokunaga, A. T., & Bernstein, M. P. 1999, ApJ, 513, 294
Pendleton, Y. J., Tielens, A. G. G. M., & Werner, M. W. 1990, ApJ, 349, 107
Persi, P., Busso, M., Corcione, L., Ferrari-Toniolo, M., & Marenzi, A. R. 1996, A&A, 306, 587
Rieke, G. H., & Lebofsky, M. J. 1985, ApJ, 288, 618
Sandford, S. A., & Allamandola, L. J. 1993, ApJ, 417, 815
Sandford, S. A., Allamandola, L. J., Tielens, A. G. G. M., & Valero, L. J. 1988, ApJ, 329, 498
Schreyer, K., Helmich, F. P., van Dishoeck, E. F., & Henning, Th. 1997, A&A, 326, 347
Schutte, W. A., Gerakines, P. A., Geballe, T. R., van Dishoeck, E. F., & Greenberg, J. M. 1996, A&A, 309, 633
Schutte, W. A., & Greenberg, J. M. 1997, A&A, 317, L43
Schutte, W. A., et al. 1998, A&A, 337, 261
Scott, G. B. I., Freeman, C. G., & McEway, M. J. 1997, MNRAS, 290, 636
Smith, R. G., Sellgren, K., & Tokunaga, A. T. 1989, ApJ, 344, 413
Snell, R. L., Scoville, N. Z., Sanders, D. B., & Erickson, N. R. 1984, ApJ, 284, 176
Strazzulla, G., Nisini, B., Leto, G., Palumbo, M. E., & Saraceno, P. 1998, A&A, 334, 1056
Taylor, S. D., Morata, O., & Williams, D. A. 1998, A&A, 336, 309
Thompson, R. I., Corbin, M. R., Young, E., & Schneider, G. 1998, ApJ, 492, L177
Ungerechts, H., Walmsley, C. M., & Winnewisser, G. 1986, A&A, 157, 207
van der Tak, F. S., van Dishoeck, E. F., Evans, N. J., II, & Blake, G. A. 1999, ApJ, 522, 991
———. 2000, ApJ, 537, 283
van Dishoeck, E. F., Wright, C. M., Cernicharo, J., Gonzalez-Alfonso, E., de Graauw, Th., Helmich, F. P., & Vandenbussche, B. 1998, ApJ, 502, L173
Waelkens, C., et al. 1996, A&A, 315, L245
Waters, L. B. R. M., Molster, F. J., & de Jong, T. 1996, A&A, 315, L361
Waters, L. B. F. M., Morris, P. W., Voors, R. H. M., & Lamers, H. J. G. L. M. 1997, in ASP Conf. Ser. 120, Luminous Blue Variables: Massive Stars in Transition, ed. A. Nota & H. J. G. L. M. Lamers (San Francisco: ASP), 326
Whittet, D. C. B., Pendleton, Y. J., Gibb, E. L., Boogert, A. C. A., Chiar, J. E., & Nummelin, A. 2001, ApJ, 550, 793
Whittet, D. C. B., Smith, R. G., Adamson, A. J., Aitken, D. K., Chiar, J. E., Kerr, T. H., Roche, P. F., Smith, C. H., & Wright, C. M. 1996, ApJ, 458, 363
Wooden, D. H., Harker, D. E., Woodward, C. E., Butner, H. M., Koike, C., Witteborn, F. C., & McMurtry, C. W. 1999, ApJ, 517, 1034
Wright, C. M., Aitken, D. K., Smith, C. H., & Roche, P. F. 1999, in Formation and Evolution of Solids in Space, ed. J. M. Greenberg & A. Li (Dordrecht: Kluwer), 77